Talanta 276 (2024) 126230

Contents lists available at ScienceDirect

Talanta

journal homepage: www.elsevier.com/locate/talanta

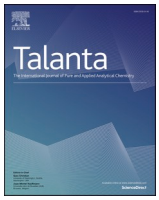

Spatial metabolomics using mass-spectrometry imaging to decipher the impact of high red meat diet on the colon metabolome in rat

Justine Ferey [a,b,1], Loïc Mervant [a,b,c,1,*], Nathalie Naud [a], Emilien L. Jamin [a,b], Fabrice Pierre [a], Laurent Debrauwer [a,b], Françoise Guéraud [a]

[a] UMR1331 Toxalim (Research Centre in Food Toxicology), Toulouse University, INRAE, ENVT, INP-Purpan, UPS, 31027, Toulouse, France
[b] Metatoul-AXIOM Platform, National Infrastructure for Metabolomics and Fluxomics, MetaboHUB, Toxalim, INRAE, 31027, Toulouse, France
[c] The Francis Crick Institute, 1 Midland Road, London, NW1 1AT, UK

ARTICLE INFO

Keywords:
Mass spectrometry imaging
timsTOF
Colonic epithelium
Red meat diet

ABSTRACT

Colorectal cancer (CRC) is the third most common cancer in the world with a higher prevalence in the developed countries, mainly caused by environmental and lifestyle factors such as diet, particularly red meat consumption. The metabolic impact of high red meat consumption on the epithelial part of the colon was investigated using Matrix-Assisted Laser Desorption/Ionization Mass Spectrometry Imaging (MSI), to specifically analyze the epithelial substructure. Ten colons from rats fed for 100 days high red or white meat diet were subjected to untargeted MSI analyses using two spatial resolutions (100 μm and 10 μm) to evaluate metabolite changes in the epithelial part and to visualize the distribution of metabolites of interest within the epithelium crypts. Our results suggest a specific effect of red meat diet on the colonic epithelium metabolism, as evidenced by an increase of purine catabolism products or depletion in glutathione pool, reinforcing the hypothesis of increased oxidative stress with red meat diet. This study also highlighted cholesterol sulfate as another up-regulated metabolite, interestingly localized at the top of the crypts. Altogether, this study demonstrates the feasibility and the added value of using MSI to decipher the effect of high red meat diet on the colonic epithelium.

1. Introduction

Over the past decade, red and processed meat consumption, conversely to white meat, has been associated with numerous adverse effects on health of which cardiovascular diseases [1], diabetes [2] and CRC [3,4] are the most frequently reported. Red meat, classified as probable carcinogen by the International Agency for Cancer Research (IARC), its constituents and neo-formed products generated during cooking, have been proposed to explain an increase in cancerous lesions observed in the colon. Therefore, due to its direct proximity with the colonic lumen and thus dietary compounds, colonic epithelium represents a relevant substructure to assess the influence of diet on the colonic tissue. Regarding CRC, a dose response relationship has been established by a meta-analysis performed by the World Cancer Research Fund that determined that a 100-g increase in red meat consumed per day was associated with a 12 % greater risk of developing CRC [5,6]. Various compounds, e.g. intrinsic to red meat or neo-formed during cooking, have been proposed as hypotheses to explain this close relationship. Neo-formed compounds such as heterocyclic aromatic amines or polycyclic aromatic hydrocarbons have been suspected to promote carcinogenesis because of their ability to form DNA adducts [7–9]. On the other hand, heme iron, present in high concentration in red meat, has been shown to promote luminal lipid peroxidation, promote the formation of preneoplastic lesions as well as reshaping the microbial community of the colonic environment [10–12]. Red meat and its constituents such as heme iron have a direct impact on the colonic epithelium as they can affect the viability of colonic epithelial cell, promote hyperproliferation and the formation of preneoplastic lesions [13]. However, little is known about the impact of red meat consumption on the colonic epithelium metabolome. Although recent studies performed on rats and pigs reported an impact of high red meat diet on the metabolome of the entire colon tissue [14,15], no study has specifically focused on the impact of this type of diet on the colonic epithelium. Thus, as this tissue is in direct contact with red meat and its constituents, analyzing specifically colonic epithelium metabolome after red meat consumption would provide direct insight into the metabolic changes induced by this consumption and could be a useful tool to decipher the

* Corresponding author. The Francis Crick Institute, 1 Midland Road, NW1 1AT, UK.
E-mail address: loic.mervant@crick.ac.uk (L. Mervant).
[1] equal contribution.

https://doi.org/10.1016/j.talanta.2024.126230
Received 25 October 2023; Received in revised form 26 April 2024; Accepted 7 May 2024
Available online 8 May 2024

Abbreviations

CRC	Colorectal cancer
IARC	International Agency for Cancer Research
MSI	Mass Spectrometry-based Imaging
LC-MS	Liquid Chromatography Mass Spectrometry
GC-MS	Gas Chromatography Mass Spectrometry
MALDI-TOF	Matrix-Assisted Laser Desorption/Ionization Time-Of-Flight
timsTOF	Trapped Ion Mobility Time-Of-Flight
DHB	2,5- Dihydroxybenzoic acid
9-AA	9-Amino-acridine
CMC	Carboxymethylcellulose
ROI	Region of Interest
HMDB	Human Metabolome DataBase
RMS	Root Mean Square
PCA	Principal Component Analysis
ROC:	Receiver Operating Characteristic
AUC	Area Under the Curve
ROS	Reactive Oxygen species

events leading to the promotion of carcinogenesis.

Due to the high prevalence of CRC, various metabolomics studies were performed to improve our understanding of the metabolic disturbance at the cancerous stage. To improve the mechanistic understanding of CRC development, many studies investigated tumoral colon or more precisely tumoral biopsies. For example, L. Nugent et al. performed metabolomic analyzes of colorectal adenoma by Liquid Chromatography Mass Spectrometry (LC-MS) and Gas Chromatography Mass Spectrometry (GC-MS) and highlighted accumulation of some metabolites as inflammatory markers, depletion of antioxidant related metabolites in adenoma biopsies [16]. Other works have focused on the influence of diet on the metabolic disruption of the gut microbiota. J. Yang and al. studied the role of high-fat diet in driving CRC and demonstrated that an elevated amount of lysophosphatidic acid promotes CRC cell proliferation [17]. Usual analytical techniques (LC, GC, capillary electrophoresis-MS …) targeted on the colon or fluids (urine, serum), were largely developed in the case of CRC study [18–20]. Few of them were dedicated to the epithelium characterization [21], notably in the case of study of influence of diet, due to the high difficulty to distinguish the different colon substructures.

Mass spectrometry imaging is a start-of-art technique in the field of tissue based-research. Hundreds to thousands of molecules can be visualized on a tissue with this label-free technique. Introduced by Caprioli et al. [22], Matrix-Assisted Laser Desorption/Ionization Time-Of-Flight (MALDI-TOF) technology has entered the field of tissue analysis by spatially imaging the mass-to-charge (m/z) ratio of both endogenous/exogenous molecules. By providing precise molecular information, this technology has attracted intense attention to complement more traditional optical imaging techniques (histology, microscopy…) in various fields such as pharmaceutical or biomedicine (cancer-based research, monitoring of drug efficiency, distribution and metabolization), allowing to investigate the metabolome in-situ and introduce spatial metabolomics [23–25]. MSI was already used for colon imaging related to CRC studies and was proved as an efficient technique for tissue profiling [21,26–28]. However, only few studies were dedicated to the investigation of the metabolome of the epithelial compartment of colon. In this way, the objective of this study was to investigate the insight of MALDI-MSI coupled to Trapped Ion Mobility Time-Of-Flight (timsTOF) Mass Spectrometry for the visualization and the identification of high red meat consumption markers within the colon epithelium in a pre-cancerous stage. In this way, a MSI workflow was optimized to perform high spatial resolution analysis, not only to regionalize the effect on the epithelial part but also to allow seeing effects within the crypt. For this biological study, 10 rats were fed either raw red or white meat for 100 days. Sample preparation was optimized to allow high spatial resolution imaging mass spectrometry (10 μm) and to visualize the localization of metabolic dietary effect within the crypt. Experiments were performed on the timsTOF fleX instrument which allows 4D-spatial Omics analysis (localization, intensity, m/z, collision cross section), visualization and identification of red meat diet markers within the crypt of the colon epithelium. In this way, this work combined various analytical and biological novelties, namely high spatial resolution MALDI imaging (10 μm), the ion mobility dimension for imaging analysis and the study of diet effect on the rat colon epithelial part with the localization of biomarkers within the crypt.

2. Materials and methods

2.1. Reagents and chemicals

All solvents and LC/MS calibration mixture were purchased from Fisher Scientific (Thermo Fisher Scientific, Illkirch, France). 2,5- Dihydroxybenzoic acid (DHB), 9-Amino-acridine (9-AA), carboxymethylcellulose (CMC) and gelatin from porcine skin were purchased from Sigma-Aldrich (St. Louis, USA).

2.2. Animal and diets

Four weeks-old male F344 rats (5 rats/group) were purchased from Charles River and housed in conventional cages. Animal experiment was authorized by the French Ministry for Higher Education, Research and Innovation (MESRI) in accordance with the local ethic committee evaluation (APAFIS#27180–2020091017209910 v2). After random assignment to cages, rats underwent a 10-days period acclimation and were fed a standard chow. After acclimatization rats were fed the experimental diets for 100 days. To initiate carcinogenesis rats were injected intraperitoneally with azoxymethane (20 mg/kg body weight) 5 days before experimental diet. Rats had unlimited access to tap water and diet throughout the experiment. Diets were provided daily in the late afternoon to limit oxidation. The red meat diet contained 40 % (on a dry weight basis) of 5 % fat beef meat (Picard, France) and white meat diet contained 40 % (on a dry weight basis) of chicken breast. White meat diet was adjusted for fat using saturated animal fat. Experimental diets composition is detailed in Table S1.

2.3. Sample collection

After 100 days of experimental diets, rats were sacrificed by exsanguination after isoflurane inhalation. Colons were harvested, washed with Phosphate Buffered Saline (PBS) solution, opened longitudinally and prepared as “swiss-rolls” (approximate dimension: *diameter* = 7 mm; *height* = 1 cm).

2.4. Tissue preparation

2.4.1. Tissue embedding

Four percent CMC solution (W/V) and 10 % gelatin solution (W/V) were prepared by dissolving the appropriate amount of powder in distilled water. For powder dissolution, solution was gently stirred to avoid air bubble and heated at 60 °C. Three different embedding techniques were tested in this work. For each Swiss-roll, 3 serial slices were cut and either embedded in CMC or gelatin prior to freezing or snap-frozen in isopentane vapors (pre-cooled with liquid nitrogen) to preserve tissue integrity.

2.4.2. Tissue sectioning

12 μm sections were cryo-sectioned using a cryostat Microm HM550 at −20 °C for both the specimen and the chamber. Sections were

mounted on conductive Indium Tin Oxide (ITO)-coated slides (Bruker, Bremen, Germany, 50 × 25 mm), vacuum dried for 15 min in a desiccator and stored at −80 °C. Before analysis, the slides were vacuum dried for 30 min in a desiccator before MALDI matrix application.

2.5. MALDI matrix deposition

The colon tissues were coated using a homogeneous automatic microsprayer HTX TM-sprayer M3 (HTX Imaging, Chapel Hill, NC, US). In this work, various matrix deposition parameters were tested for DHB application and optimization results are summarized in Table S2 and Fig. S2.

2.6. Mass spectrometry instrumentation

MALDI imaging analyses were performed on a timsTOF fleX instrument (Bruker Daltonics, Bremen, Germany) equipped with both laser desorption ionization source (Smartbeam 3D laser technology, Bruker Daltonics, Bremen, Germany) and an electrospray ionization (ESI) source. MALDI mass spectrometry analyses were performed in both positive and negative ionization modes in the *m/z* range 100–1000 with trapped ion mobility switched off. Analyses were performed with a 10-kHz laser and each pixel was the result of 200 laser shots. Entire swiss-roll were acquired at 100 µm spatial resolution. For all colon, Region Of Interest (ROI) were then acquired at 10 µm spatial resolution. Only one swiss-roll was profiled at 100 µm with the trapped ion mobility switched on to evaluate the spatial distribution of isomeric/isobaric compounds of interest.

Before each analysis, external calibration was performed in the suitable ionization mode by Tuning-Mix infusion via the ESI source in the *m/z* range 100–1000. For Ion mobility analyses, spectra were scanned from 1/K0 0.63 V.s.cm^{-2} to 1/K0 1.70 V.s.cm^{-2} with a ramp time at 50 ms and an accumulation time at 20 ms.

2.7. Data processing

2.7.1. Processing

Images were acquired with the timsControl (Bruker, Bremen) and FlexImaging (version 5.1, Bruker, Bremen) softwares. Images were then processed with SCiLS Lab Pro, TIMS Data Viewer and DataAnalysis (version 5.3) softwares (Bruker Daltonics, Bremen, Germany). Pathway enrichment analysis was performed using MetaboAnalyst 5.0 [29] and false discovery rate was used to correct for p-value. ROC curve and AUC calculation were performed using SCiLS Lab Pro.

2.7.2. Metabolite annotation

A preliminary annotation of all the features was performed using HMDB database with a threshold of ± 10 ppm. To increase confidence in annotations, putatively annotated metabolites were fragmented via « on-tissue » tandem mass spectrometry MALDI MS/MS experiments. Ions of interest were isolated using a ± 2 Da window and fragmented by Collision-Induced Dissociation with energy levels between 10 and 40 eV. Spectra were recalibrated using the single point calibration option and reprocessed using DataAnalysis (version 5.3) software (Bruker Daltonics, Bremen, Germany). Experimental MS/MS spectra were compared with MS/MS data from both the HMDB open source database [30] and the MetFrag in-silico fragmentation tool [31]. Annotation displayed in this manuscript constitute a level 2 annotation according to the Metabolomics Standard Initiative guidelines [32].

3. Results

3.1. Sample preparation

3.1.1. Tissue embedding

Tissue preparation is of significant importance to obtain high quality image in mass spectrometry imaging, combining high spatial resolution and analytical sensitivity. Tissues must not be damaged during sampling, conditioning, preservation and during the MALDI matrix deposition stages. To this aim, all these steps must be optimized to study the localization of metabolites in small tissue regions, namely the crypts of rat colons. Collected tissues can either be directly snap-frozen or embedded in MSI compatible media before freezing. In this work, three sampling methods were tested, namely snap-freezing, and embedding in carboxymethylcellulose (4 % w/w) or gelatin (10 % w/w). Theses embedding matrices are commonly used in MSI experiments to prevent tissue degradation and to facilitate cutting. During the sampling process, colons were prepared as swiss-rolls by cutting them longitudinally then rolling it up in itself. Tissues were then frozen in isopentane (cooled with liquid nitrogen) according to the three conditions mentioned above.

The impact of sample preparation on analytical sensitivity was evaluated. For that, the signal intensities, normalized to Root Mean Square (RMS) for each condition, were compared within the *m/z* 100–1000 range. For each condition, three consecutive slices were analyzed with the timsTOF mass spectrometer at the 100 µm spatial resolution. Only the *m/z* peaks retrieved in the three conditions were selected for data processing. The means of the signal intensities medians were calculated in triplicate (n = 3) by dividing the *m/z* range. As shown in Fig. S1 (a), the frozen condition appeared to give higher sensitivity in the low *m/z* region whereas CMC condition led to higher intensities in the *m/z* 600–1000 range. Results obtained with gelatin embedding showed globally lower intensities over all the *m/z* range.

The annotation capacity was also evaluated. For the three conditions, each *m/z* values extracted from SciLS software was matched with internal and public databases (HMDB, Lipid Maps) using a 15 ppm mass error tolerance. For each embedding, only peaks showing less than 25 % variability for n = 3 were kept for the test. Results are illustrated in the Venn diagram presented in Fig. S1 (c). The gelatin embedding yielded the higher number of matches with 752 hits against 719 for the snap-frozen condition and 729 for the CMC embedding media, after variability filtration. This result may be due to the higher variability of the snap-frozen condition with 23 % of peak intensities showing more than 25 % of variability (Coefficient of Variation, CV > 25 %, n = 3) against CV = 13 % and CV = 16 % for CMC and gelatin conditions respectively. Considering the mass range, snap-frozen condition yielded more hits in the *m/z* range of 200–500. Spatial resolution obtained after MSI analyses did not allow to discriminate the three conditions (no delocalization detected). Therefore, the snap-frozen condition was chosen as the best compromise to limit tissue preparation steps, to avoid signals originating from the embedding matrix or sample preparation and to maximize annotation capacity in the low *m/z* range.

3.1.2. DHB matrix deposition method

In the positive ionization mode, DHB matrix was chosen thanks to its range of molecular weights application (metabolites, lipids). Matrix deposition process is of great importance to obtain high quality image showing the biological spatiality of metabolites of interest. This step must allow efficient molecule extraction for high desorption/ionization process while reducing metabolite delocalization. Various deposition parameters, presented in Table S2, were tested (matrix concentration, solvent, flow rate, number of passes) for the positive ionization mode. Two over the 4 matrix deposition methods (namely A and C, Table S2) were described in the literature for the analysis of biological tissues including colon [33,34]. In particular, method C has already been used to visualize the distribution of drug in the intestine, along the crypt-villus axis at 5 µm spatial resolution by MALDI-MSI [33]. Fig. S2 shows DHB crystallization using the four deposition methods. Method B (*Flow rate* = 0.1 mL min^{-1}; *Number of passes* = 14; *Track spacing* = 3 mm; *Nozzle temperature* = 60 °C; *Nozzle velocity* = 1200 mm; *N2 pressure* = 10 psi) clearly shows the lowest granulometry. This method was selected for this study to reach optimal spatial resolution within the villus-crypt. For negative ionization mode, the deposition procedure with 9-AA used

in the lab proved to be compatible with high resolution imaging analysis as it yielded low granulometry and no spatial delocalization of metabolites.

3.2. Imaging mass spectrometry method

3.2.1. Repeatability

Repeatability of MSI on the timsTOF instrument was evaluated. Low analytical variability is required to obtain high confidence annotation for biological interpretation. In this context, 9 serial swiss-roll slices were analyzed over 3 days (n = 3 per day). Variability was assessed by estimating the number of ions exhibiting CV > 25 %. For each replicate, only ions detected in all the replicates (inter and intra-day) were processed. Results are summarized in Table 1. The intra-day study (n = 3) showed quite low variability (below 21 %) for MSI analysis whereas inter-day variability was higher with 37 % ions intensities showing CV > 25 %. This variability may be attributed to either sample preparation variability (matrix deposition) or analytical variability over days. It should also be noted that the inter-day is calculated using 9 replicates whereas intra-day variability uses only 3. Given this observation, the analyses were then performed on the same day to limit this higher inter-day variability. Moreover, the scan rate of the MSI ToF MS analysis (around 15 pixels.s^{-1} in our analytical conditions) allowed the analyses to be carried out on the same day. The matrix deposition was performed simultaneously for all the sections and the tissue analysis was carried out randomly between the two diet conditions.

3.2.2. Spatial resolution influence

This work focused on the set up of an MSI analytical method to study the impact of red meat consumption on the colonic epithelium metabolome. Therefore, the objective of this method development was not only to regionalize the effect on the epithelial part but also to see effects within the crypts. The first step was to confirm the potential of the analytical method to regionalize the epithelial part of the colon. A 100 μm spatial resolution analysis was therefore performed over the entire swiss-roll sample. The image was imported into SCiLS Lab software and was subjected to unsupervised segmentation (hierarchical clustering). As shown in Fig. 1 (a), 100 μm spatial resolution is sufficient to allow segmenting the tissue substructures and thus to distinguish the epithelial part. In a second step, to visualize metabolite distribution within the crypts, various spatial resolutions (namely 10 μm, 20 μm and 50 μm) were tested to find the best compromise between metabolites visualization and analytical sensitivity. A spatial resolution above 10 μm did not allow to precisely spatially resolve the crypt of the epithelium. As shown in Fig. 1 (b, c), 10 μm spatial resolution analysis allowed to visualize the crypts highlighting a molecular gradient. This study was therefore performed at two different spatial resolutions. First, a tissue profiling of the entire swiss-roll was carried out at 100 μm spatial resolution to highlight discriminative metabolites between the two groups within the epithelium compartment. Then, the distribution within the crypt of metabolites of interest was visualized using a 10 μm spatial resolution analyses on a small part of the swiss-roll.

Table 1
Intra-day (n = 3) and inter-day (n = 3) variabilities of swiss-roll MALDI MSI analysis.

	Intra-day variability			Inter-day variability
	Day 1 (n = 3)	Day 2 (n = 3)	Day 3 (n = 3)	D1+D2+D3 (n = 9)
Number of peaks	1869	1869	1869	1869
Number of peaks with intensities CV > 25 %	**18 %**	**15 %**	**21 %**	**37 %**

3.3. Biological results

This work explored the differential metabolic patterns between colons from rats fed two different diets (either red meat/beef or white meat/chicken). After MSI acquisition, data were imported into SCiLS software and were normalized to RMS. Colons were segmented using hierarchical clustering algorithm to regroup pixels in clusters defining biochemical zones and submitted to multivariate analysis (Principal Component Analysis). Fig. 2 shows a segmented swiss-roll and the associated PCA analysis in the positive ionization mode highlighting two principal biological zones: epithelial (blue) and muscular (yellow). The red compartment is a non-tissue zone generated during the rolling up of the swiss-roll. The hierarchical segmentation was applied to each swiss-roll sample to select the epithelial zones which were subjected to unsupervised PCA analysis using the Min-Max scaling. The PCA scores plots for both ionization mode presented in Fig. S3 show a discrimination of the two groups (green: chicken diet, red: beef diet) suggesting molecular differences in the epithelium between the two diets.

To visualize diet effects on the regionalized epithelial part, Receiver Operating Characteristic (ROC) test was then applied on the features detected in the epithelial tissue to highlight the discriminating metabolites between the two diets. Ions with Area Under the Curve (AUC) values higher than 0.7 (or lower than 0.3) were selected as discriminative. In a second step, to evaluate the impact of the diet within the epithelial crypt, the epithelium tissue was subjected to another segmentation by hierarchical clustering followed by a ROC test comparing features detected at the top or the bottom of the crypt. Fig. S4 shows a different spectral area located at the top of the crypt (blue zone). This result suggested that some metabolites are specifically localized at the top of the crypt. Fig. 3 (a) and (b) shows AUC values for discriminant metabolites localized in the epithelial part and at the top of the crypts, respectively. As presented in Fig. 3, 22 metabolites were found discriminant, respectively 19 in the negative ionization mode and 3 in the positive mode. These metabolites were first assigned using the open source HMDB database [30], using a tolerance of ± 10 ppm. Next, structural elucidation was confirmed via « on-tissue » tandem mass spectrometry MALDI MS/MS experiments.

The online MetFrag tool [31] was used to generate in-silico fragmentation profiles of the possible candidates. Other MS/MS spectra were compared to data available on the online HMDB database. Annotated metabolites are summarized in Table 2. Mass spectra acquired in MSI revealed low mass error measurements (below 8 ppm) which is highly acceptable for this instrument technology concerning imaging analyses.

The *m/z* 465.3065 ion was particularly interesting due to its higher AUC value at the top of the crypt (0.71 at the top *versus* 0.66 in whole epithelium) from rats fed red meat. The distribution of this ion for both 100 μm and 10 μm studies with the associated ROC curve are displayed in Fig. 4. This ion was annotated by generation of the molecular formula (mass accuracy, isotopic pattern), *m/z* comparison with the HMDB spectral library, MS/MS experiments and CCS value measurement with ion mobility experiments. First, the molecular formula of the ion of interest was determined using mass accuracy from both the monoisotopic peak and the isotopic profile. The monoisotopic peak detected at *m/z* 465.3065 displayed 7 candidate formulas below 10 ppm mass error. Combining this high-resolution measurement with the study of the isotopic pattern (Fig. S5) the molecular formula $C_{27}H_{46}O_4S$ $[M-H]^-$ was selected (mσ 4.8, *m/z* error 2.3 ppm). According to the open source HMDB database, cholesterol sulfate was proposed. Assignment was reinforced with an ion mobility mass spectrometry imaging analysis. An entire swiss roll was analyzed at 100 μm spatial resolution with the mobility cell activated. For the *m/z* 465.3065, two ions were detected at 1/K0 = 1.055 and 1/K0 = 1.165, corresponding to CCS values of 218 $Å^2$ and 240 $Å^2$ respectively. As shown in Fig. S6, the *m/z* 465.3065 ion (with CCS 240 $Å^2$) is located at the top of the crypt. This CCS measurement reinforced the assignment of cholesterol sulfate with an error

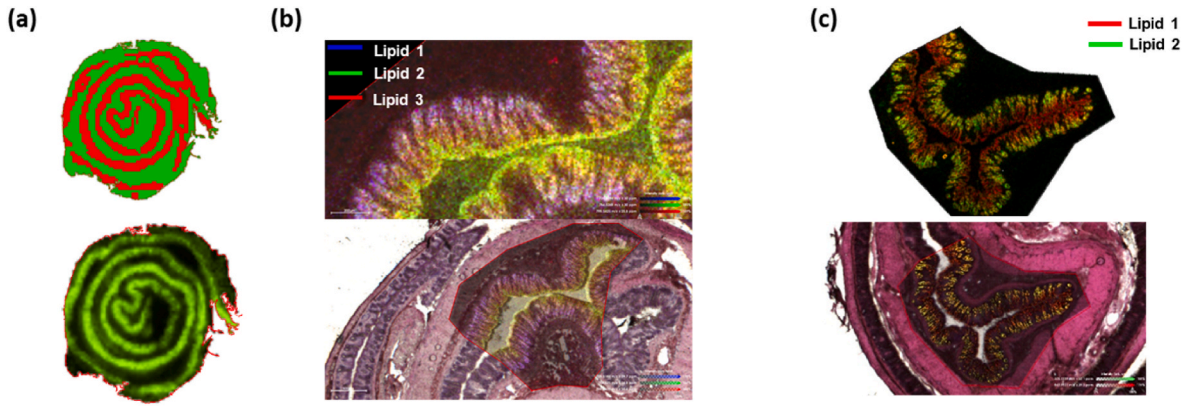

Fig. 1. (a) Segmented swiss-roll at 100 μm spatial resolution, highlight of the epithelial tissue, (b) MSI image of the epithelium at 10 μm spatial resolution in the positive ionization mode using DHB matrix, (c) MSI image of the epithelium at 10 μm spatial resolution in the negative ionization mode using 9-AA matrix.

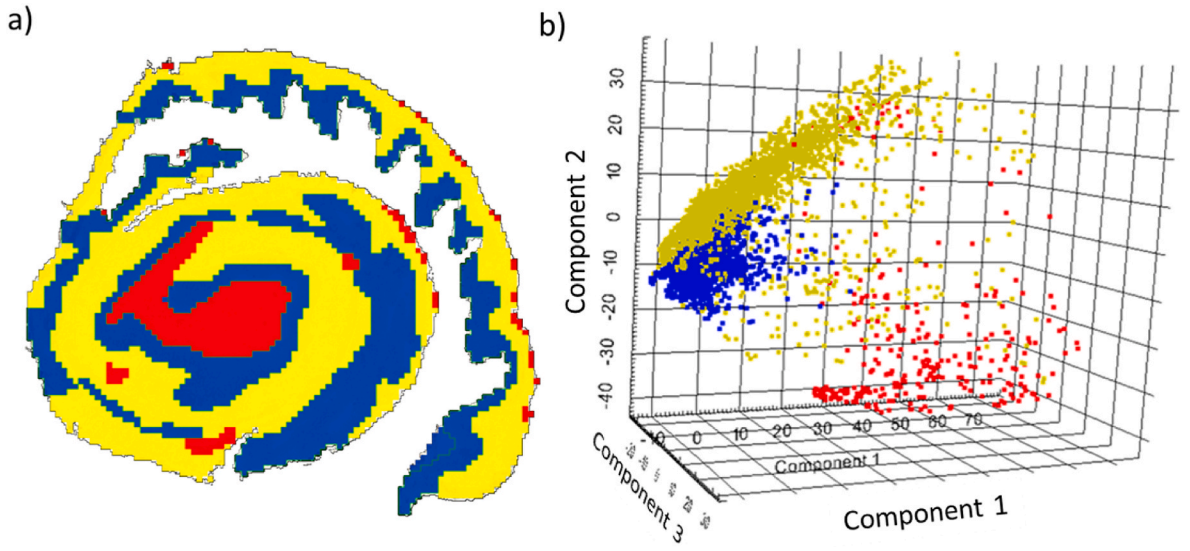

Fig. 2. (a) Segmented swiss-roll at 100 μm spatial resolution, (b) associated Principal Component Analysis.

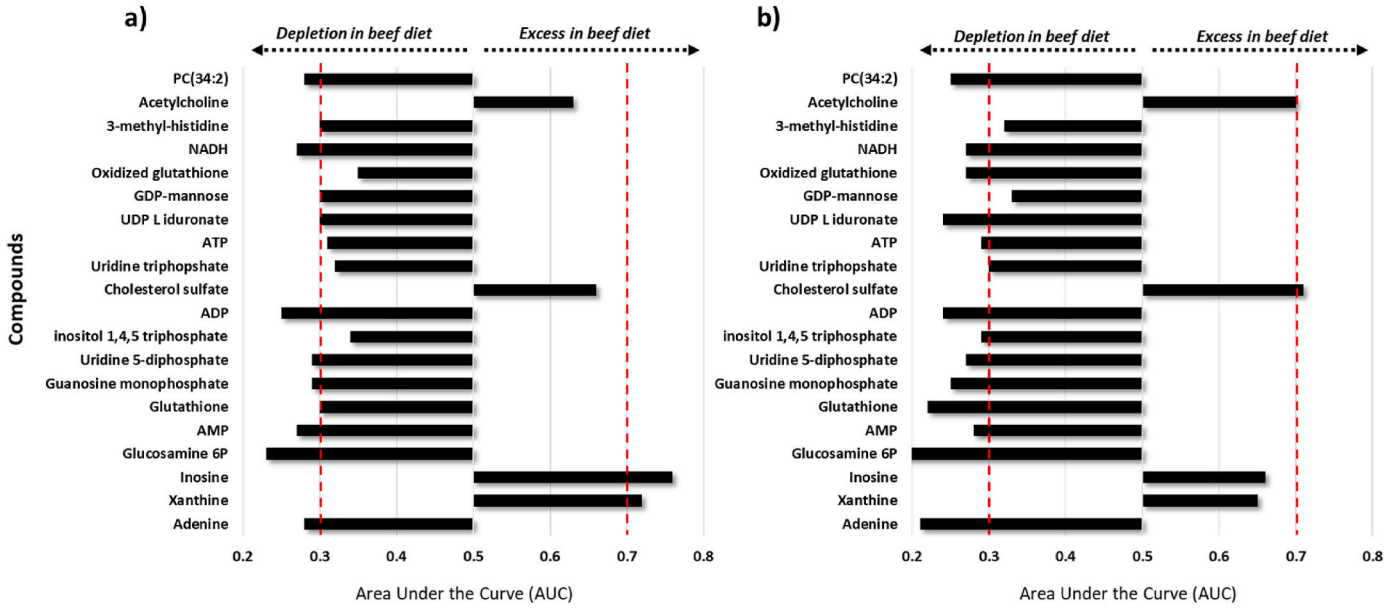

Fig. 3. Area Under the Curve (AUC) values of discriminant metabolites between red and white meat diets for (a) the epithelium part and for (b) the top of the crypts.

Table 2
Discriminant annotated metabolites associated with their Area Under the Curve (AUC) values and mass accuracies.

Experimental *m/z*	AUC (beef versus chicken)		Annotation	Raw formula	Adduct	Mass accuracy ppm
	Crypts	Top of the crypts				
134.0476	0.28	0.21	Adenine	$C_5H_5N_5$	$[M-H]^-$	2.8
151.0248	0.72	0.65	Xanthine	$C_5H_4N_4O_2$	$[M-H]^-$	8.9
267.072	0.76	0.66	Inosine	$C_{10}H_{12}N_4O_5$	$[M-H]^-$	5.6
280.022	0.23	0.18	Glucosamine 6P	$C_6H_{14}NO_8P$	$[M+Na-2H]^-$	5.8
328.0424	0.27	0.28	AMP	$C_{10}H_{14}N_5O_7P$	$[M\text{-}H2O\text{–}H]^-$	8.7
344.0348	0.3	0.22	Glutathione	$C_{10}H_{17}N_3O_6S$	$[M+K-2H]^-$	6.9
362.0537	0.29	0.25	Guanosine monophosphate	$C_{10}H_{14}N_5O_8P$	$[M-H]^-$	8.2
402.9923	0.29	0.27	Uridine 5-diphosphate	$C_9H_{14}N_2O_{12}P_2$	$[M-H]^-$	6.5
418.9566	0.34	0.29	inositol 1,4,5 triphosphate	$C_6H_{15}O_{15}P_3$	$[M-H]^-$	3.6
426.0226	0.25	0.24	ADP	$C_{10}H_{15}N_5O_{10}P_2$	$[M-H]^-$	1.1
465.3065	0.66	0.71	Cholesterol sulfate	$C_{27}H_{46}O_4S$	$[M-H]^-$	4.5
482.964	0.32	0.3	Uridine triphopshate	$C_9H_{15}N_2O_{15}P_3$	$[M-H]^-$	5.7
505.99	0.31	0.29	ATP	$C_{10}H_{16}N_5O_{13}P_3$	$[M-H]^-$	3
579.0227	0.3	0.24	UDP L iduronate	$C_{15}H_{22}N_2O_{18}P_2$	$[M-H]^-$	7.4
604.0709	0.3	0.33	GDP-mannose	$C_{16}H_{25}N_5O_{16}P_2$	$[M-H]^-$	1.7
611.1495	0.35	0.27	Oxidized glutathione	$C_{20}H_{32}N_6O_{12}S_2$	$[M-H]^-$	7.9
664.1221	0.27	0.27	NADH	$C_{21}H_{29}N_7O_{14}P_2$	$[M-H]^-$	6.9
170.0933	0.3	0.32	3-methyl-histidine	$C_7H_{11}N_3O_2$	$[M+H]^+$	5.3
146.1175	0.63	0.7	Acetylcholine	$C_7H_{16}NO_2$	$[M+H]^+$	0.4
796.5286	0.28	0.25	PC(34:2)	$C_{42}H_{80}NO_8P$	$[M+K]^+$	4.1

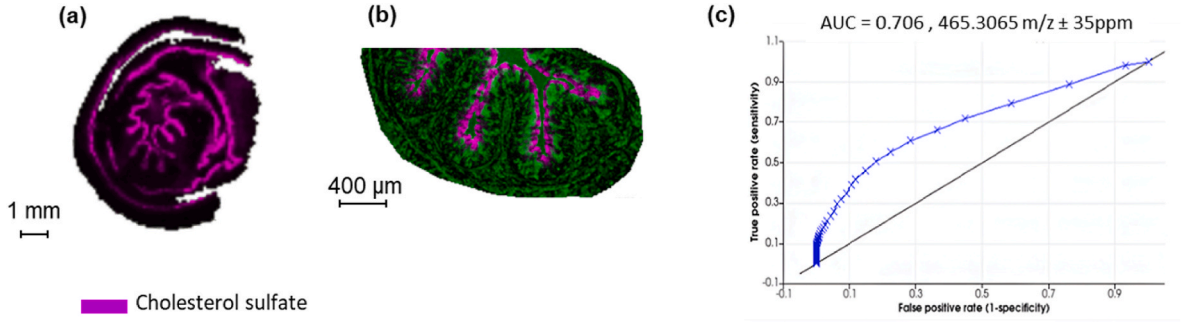

Fig. 4. Visualization of cholesterol sulfate (a) over the swiss-roll at 100 µm spatial resolution, (b) within the epithelium at 10 µm spatial resolution associated with (c) the Receiver Operating characteristic (ROC) curve of red versus white meat diet.

of 3.5 % (LipidCCS Zhu Lab [35]). Assignment was also confirmed by a MS/MS spectrum acquisition, highlighting the diagnostic fragment ion $[SO_4H_2\text{–}H]^-$ at *m/z* 96.952.

4. Discussion

MSI has already been applied to study the influence of diet on the metabolome/lipidome of a tissue [36–38] including a study concerning the influence of a high fat diet on mouse intestine [39]. Furthermore, various MSI works were carried out on intestine tissue to evaluate the molecular content of tumoral regions [21,26,27]. However, to the best of our knowledge, there is no work in the literature concerning the study of the impact of high red meat consumption on the metabolome of crypt-villus tissue.

By using MSI we were able to spatially resolve all substructures of the colonic environment in order to concentrate on a specific tissue as the epithelium. A 100 µm spatial resolution analysis enabled to segment the tissue and to distinguish the epithelial part. The comparison of the epithelia between the two diet groups highlighted some discriminative metabolites with higher analytical sensitivity than at a 10 µm spatial resolution. These analyses, performed on the timsTOF instrument offered fast MS imaging capacities (at 15 pixel.s^{-1}, meaning around 7 min for 6000 swiss-roll pixels), allowing analyses to be carried out on a single day and avoiding additional instrumental variability. Moreover, sample preparation optimizations allowed to perform high spatial resolution TOF-MS imaging and to visualize the distribution of the discriminative metabolites within the crypts. Few studies showed similar resolution on the epithelial part using TOF-MS instruments [33,40,41]. Besides, the use of ion mobility dimension enabled the separation of cholesterol sulfate isomer/isobar and CCS measurement and helped to increase the reliability of the annotation.

In this work, we explored the differential metabolic patterns of colon samples from rats fed red or white meat. Our results showed metabolic pathways remodeling in the colon of rats fed red meat with discriminative metabolites found to be up and downregulated. A pathway enrichment analysis, shown in Fig. 5, revealed that, among impacted pathways in the colonic epithelium, purine catabolism was one of the most disturbed by the high red meat diet.

This leads to an increase of final products of the purine catabolism pathway such as inosine, xanthine and hypoxanthine and a decrease of purine related levels such as IMP and AMP as shown in Fig. 6. This result could be explained by the high amount of iron (in particular heme-iron) contained in red meat conversely to white meat diet. Indeed, numerous studies have shown that iron was an activator of purine catabolism and in particular of xanthine oxidase [42–44]. Such activation of xanthine oxidase activity leads to an increase of hydrogen peroxide and oxygen superoxide which may induce oxidative stress [43]. These data suggest that, in addition to the extensively described heme-induced lipid peroxidation [45–47], heme iron could also impact the metabolism of the colonic epithelium leading to the generation of Reactive Oxygen Species (ROS) and thus contributing to the formation of a pro-oxidative environment. This hypothesis is also supported by the lower levels of glutathione (both oxidized and reduced) detected in the epithelium of the colon of rats fed with high red meat diet, suggesting higher

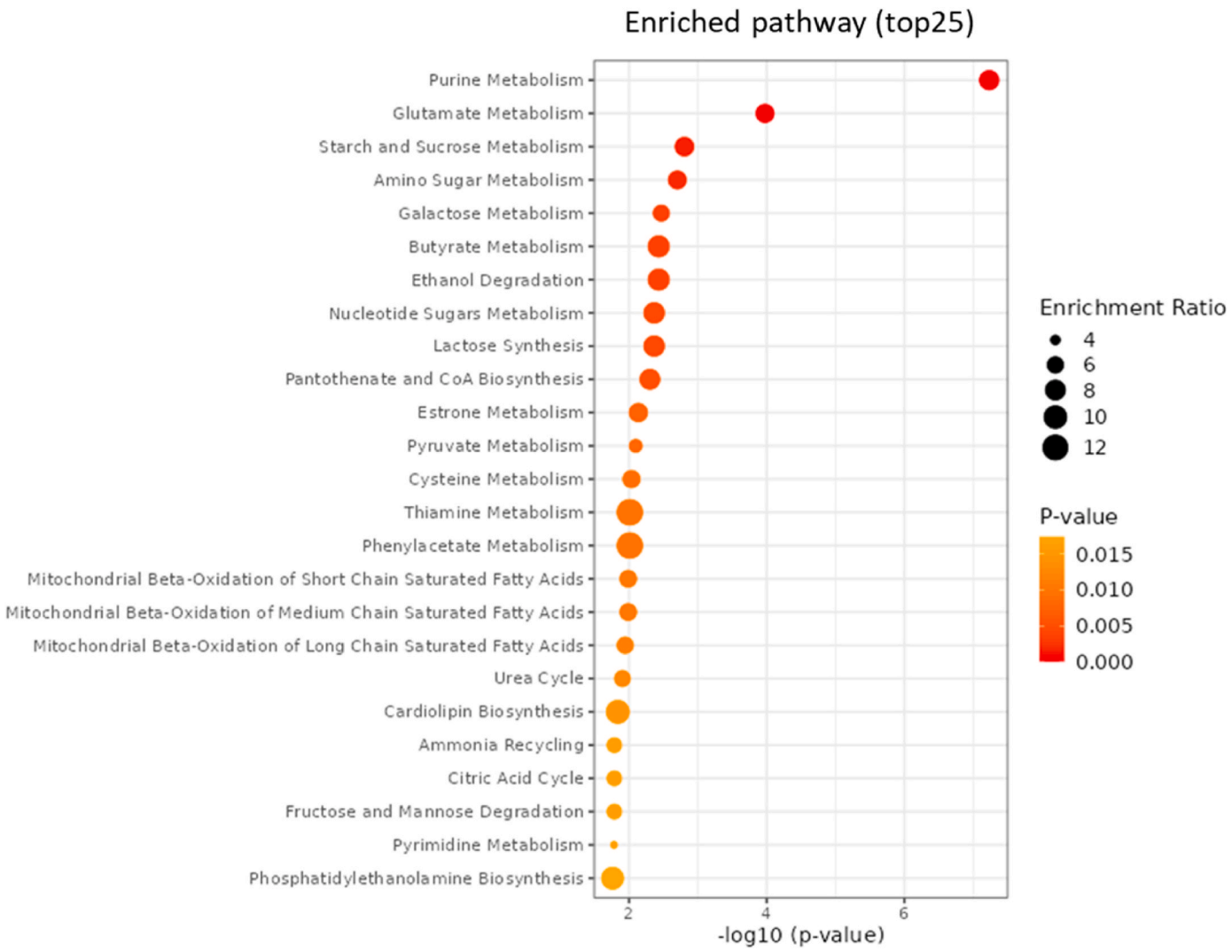

Fig. 5. Visualization of top 25 significant pathways.

consumption of glutathione for the removal of ROS and lipid peroxidation products, such as 4-hydroxynonenal.

In addition of deciphering the impact of red meat consumption specifically on the colonic epithelium, the developed method allowed us to identify effects within the colonic crypts. In particular we were able to highlight specific localization of cholesterol sulfate at the border of the crypts and an excess of this compound in rats fed high red meat diet. Interestingly, cholesterol sulfate has been shown as an essential compound for the binding of the matrix metalloproteinase-7 (MMP-7) [48, 49]. Yamamoto and colleagues demonstrated that by cleaving extra-cellular protein and cell-surface protein MMP-7 facilitates the invasion and the aggregation of cancer cells in the colon [48]. Therefore, a question can be raised concerning the role of cholesterol sulfate in the tumoral progression.

Together, these results highlight the potential of MSI to spatially resolve the dietary-induced metabolic changes in the colonic environment. As it is in direct contact with the colonic lumen and the diet constituents, the colonic epithelium constitutes a vulnerable matrix to deleterious effect induced by the diet.

5. Conclusion

To our knowledge, this study is the first work using MSI to evaluate the influence of diet on colon epithelium metabolome, showing specific distribution of metabolites within the crypt-villus. The timsTOF technology offered various advantages such as speed of analysis, high spatial resolution as well as ion mobility dimensions. This last technology enabled to distinguish two isobaric metabolites, one of which is of major interest in our study. It was found upregulated in the epithelium of rat fed red meat diet and spatially localized at the top of the crypt. Moreover, this methodological development allowed to reveal some disrupted metabolic pathways, in particular purine and glutathione metabolism pathways, shown to be impacted by high red meat diet. In conclusion, this work could provide additional spatial information to set the stage for a better understanding of the effect of dietary intake on the colonic metabolome.

CRediT authorship contribution statement

Justine Ferey: Conceptualization, Data curation, Formal analysis, Investigation, Methodology, Writing – original draft, Writing – review & editing. **Loïc Mervant:** Conceptualization, Data curation, Formal analysis, Investigation, Writing – original draft, Writing – review & editing. **Nathalie Naud:** Investigation, Resources. **Emilien L. Jamin:** Resources, Writing – review & editing. **Fabrice Pierre:** Funding acquisition, Resources, Writing – review & editing. **Laurent Debrauwer:** Conceptualization, Funding acquisition, Resources, Supervision, Writing – review & editing. **Françoise Guéraud:** Conceptualization, Funding acquisition,

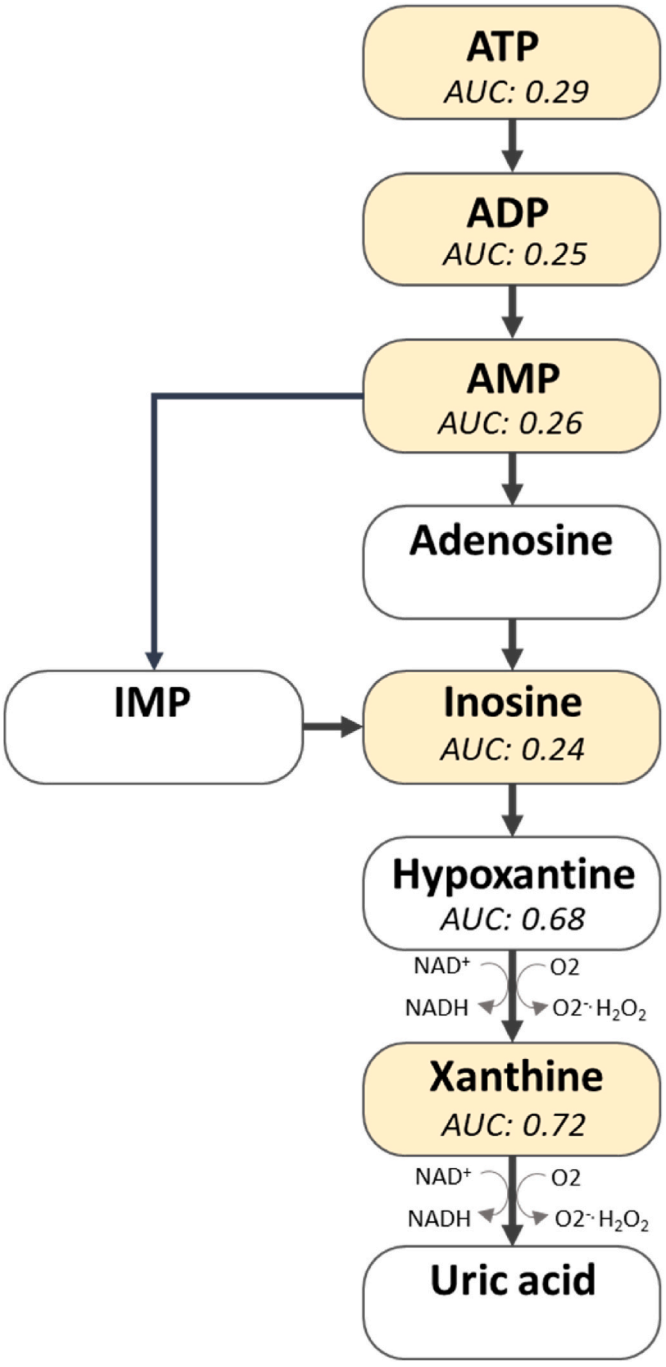

Fig. 6. Purine catabolism pathway.

Resources, Writing – review & editing.

Declaration of competing interest

The authors declare that they have no known competing financial interests or personal relationships that could have appeared to influence the work reported in this paper.

Data availability

Data will be made available on request.

Acknowledgment

Sources of support for the work: PhD doctoral fellowship of LM was co-funded by INRAE (Nutrition, Chemical Food Safety and Consumer Behaviour Scientific Division) and French region Occitanie. All MS experiments were performed on the instruments of the MetaToul-AXIOM platform, partner of the national infrastructure of metabolomics and fluxomics: MetaboHUB [MetaboHUB-ANR-11-INBS-0010, 2011]. This work has been funded by the "Institut National du Cancer" (INCA_12705)-Project PLBIO18-130 and approved by the "Réseau NACRe".

Appendix A. Supplementary data

Supplementary data to this article can be found online at https://doi.org/10.1016/j.talanta.2024.126230.

References

[1] C.S. Kwok, M. Gulati, E.D. Michos, J. Potts, P. Wu, L. Watson, Y.K. Loke, C. Mallen, M.A. Mamas, Dietary components and risk of cardiovascular disease and all-cause mortality: a review of evidence from meta-analyses, Eur. J. Prev. Cardiol. 26 (2019) 1415–1429, https://doi.org/10.1177/2047487319843667.

[2] M. Kouvari, V. Notara, N. Kalogeropoulos, D.B. Panagiotakos, Diabetes mellitus associated with processed and unprocessed red meat: an overview, Int. J. Food Sci. Nutr. 67 (2016) 735–743, https://doi.org/10.1080/09637486.2016.1197187.

[3] G. Grosso, S. La Vignera, R.A. Condorelli, J. Godos, S. Marventano, M. Tieri, F. Ghelfi, L. Titta, A. Lafranconi, A. Gambera, E. Alonzo, S. Sciacca, S. Buscemi, S. Ray, D. Del Rio, F. Galvano, Total, red and processed meat consumption and human health: an umbrella review of observational studies, Int. J. Food Sci. Nutr. (2022) 1–12, https://doi.org/10.1080/09637486.2022.2050996.

[4] M.S. Farvid, E. Sidahmed, N.D. Spence, K. Mante Angua, B.A. Rosner, J.B. Barnett, Consumption of red meat and processed meat and cancer incidence: a systematic review and meta-analysis of prospective studies, Eur. J. Epidemiol. 36 (2021) 937–951, https://doi.org/10.1007/s10654-021-00741-9.

[5] W. Wcrf, World Cancer Reasearch Fund/American Institute for Cancer Research. Continuous Update Project Expert Report 2018. Meat, Fish and Daity Products and the Risk of Cancer, 2018 dietandcancerreport.org.

[6] A. Wolk, Potential health hazards of eating red meat, J. Intern. Med. 281 (2017) 106–122, https://doi.org/10.1111/joim.12543.

[7] L. Einaudi, B. Courbiere, V. Tassistro, C. Prevot, I. Sari-Minodier, T. Orsiere, J. Perrin, In vivo exposure to benzo(a)pyrene induces significant DNA damage in mouse oocytes and cumulus cells, Hum. Reprod. 29 (2014) 548–554, https://doi.org/10.1093/humrep/det439.

[8] S. Muthusamy, C. Peng, J.C. Ng, Genotoxicity evaluation of multi-component mixtures of polyaromatic hydrocarbons (PAHs), arsenic, cadmium, and lead using flow cytometry based micronucleus test in HepG2 cells, Mutat. Res. Toxicol. Environ. Mutagen. 827 (2018) 9–18, https://doi.org/10.1016/j.mrgentox.2018.01.002.

[9] R.J. Turesky, L. Le Marchand, Metabolism and biomarkers of heterocyclic aromatic amines in molecular epidemiology studies: lessons learned from aromatic amines, Chem. Res. Toxicol. 24 (2011) 1169–1214, https://doi.org/10.1021/tx200135s.

[10] N.M. Bastide, F. Chenni, M. Audebert, R.L. Santarelli, S. Taché, N. Naud, M. Baradat, I. Jouanin, R. Surya, D.A. Hobbs, G.G. Kuhnle, I. Raymond-Letron, F. Gueraud, D.E. Corpet, F.H.F. Pierre, A central role for heme iron in colon carcinogenesis associated with red meat intake, Cancer Res. 75 (2015) 870–879, https://doi.org/10.1158/0008-5472.CAN-14-2554.

[11] F. Guéraud, S. Taché, J.-P. Steghens, L. Milkovic, S. Borovic-Sunjic, N. Zarkovic, E. Gaultier, N. Naud, C. Héliès-Toussaint, F. Pierre, N. Priymenko, Dietary polyunsaturated fatty acids and heme iron induce oxidative stress biomarkers and a cancer promoting environment in the colon of rats, Free Radic. Biol. Med. 83 (2015) 192–200, https://doi.org/10.1016/j.freeradbiomed.2015.02.023.

[12] O.C.B. Martin, M. Olier, S. Ellero-Simatos, N. Naud, J. Dupuy, L. Huc, S. Taché, V. Graillot, M. Levêque, V. Bézirard, C. Héliès-Toussaint, F.B.Y. Estrada, V. Tondereau, Y. Lippi, C. Naylies, L. Peyriga, C. Canlet, A.M. Davila, F. Blachier, L. Ferrier, E. Boutet-Robinet, F. Guéraud, V. Théodorou, F.H.F. Pierre, Haem iron reshapes colonic luminal environment: impact on mucosal homeostasis and microbiome through aldehyde formation, Microbiome 7 (2019) 72, https://doi.org/10.1186/s40168-019-0685-7.

[13] F. Blachier, M. Beaumont, M. Andriamihaja, A.-M. Davila, A. Lan, M. Grauso, L. Armand, R. Benamouzig, D. Tomé, Changes in the luminal environment of the colonic epithelial cells and physiopathological consequences, Am. J. Pathol. 187 (2017) 476–486, https://doi.org/10.1016/j.ajpath.2016.11.015.

[14] C. Rombouts, L. Van Meulebroek, M. De Spiegeleer, S. Goethals, T. Van Hecke, S. De Smet, W.H. De Vos, L. Vanhaecke, Untargeted metabolomics reveals elevated L-carnitine metabolism in pig and rat colon tissue following red versus white meat intake, Mol. Nutr. Food Res. 65 (2021) 2000463, https://doi.org/10.1002/mnfr.202000463.

[15] S. Goethals, C. Rombouts, L.Y. Hemeryck, L. Van Meulebroek, T. Van Hecke, E. Vossen, J. Van Camp, S. De Smet, L. Vanhaecke, Untargeted metabolomics to

reveal red versus white meat-associated gut metabolites in a prudent and western dietary context, Mol. Nutr. Food Res. 64 (2020) e2000070, https://doi.org/10.1002/mnfr.202000070.
[16] J.L. Nugent, A.N. McCoy, C.J. Addamo, W. Jia, R.S. Sandler, T.O. Keku, Altered tissue metabolites correlate with microbial dysbiosis in colorectal adenomas, J. Proteome Res. 13 (2014) 1921–1929, https://doi.org/10.1021/pr4009783.
[17] J. Yang, H. Wei, Y. Zhou, C.-H. Szeto, C. Li, Y. Lin, O.O. Coker, H.C.H. Lau, A.W. H. Chan, J.J.Y. Sung, J. Yu, High-fat diet promotes colorectal tumorigenesis through modulating gut microbiota and metabolites, Gastroenterology 162 (2022) 135–149.e2, https://doi.org/10.1053/j.gastro.2021.08.041.
[18] Z. Long, J. Zhou, K. Xie, Z. Wu, H. Yin, V. Daria, J. Tian, N. Zhang, L. Li, Y. Zhao, F. Wang, M. Wang, Y. Cui, Metabolomic markers of colorectal tumor with different clinicopathological features, Front. Oncol. 10 (2020) 981, https://doi.org/10.3389/fonc.2020.00981.
[19] R. Udo, K. Katsumata, H. Kuwabara, M. Enomoto, T. Ishizaki, M. Sunamura, Y. Nagakawa, R. Soya, M. Sugimoto, A. Tsuchida, Urinary charged metabolite profiling of colorectal cancer using capillary electrophoresis-mass spectrometry, Sci. Rep. 10 (2020) 21057, https://doi.org/10.1038/s41598-020-78038-2.
[20] J. Wu, M. Wu, Q. Wu, Identification of potential metabolite markers for colon cancer and rectal cancer using serum metabolomics, J. Clin. Lab. Anal. 34 (2020) e23333, https://doi.org/10.1002/jcla.23333.
[21] R. Mirnezami, K. Spagou, P.A. Vorkas, M.R. Lewis, J. Kinross, E. Want, H. Shion, R. D. Goldin, A. Darzi, Z. Takats, E. Holmes, O. Cloarec, J.K. Nicholson, Chemical mapping of the colorectal cancer microenvironment via MALDI imaging mass spectrometry (MALDI-MSI) reveals novel cancer-associated field effects, Mol. Oncol. 8 (2014) 39–49, https://doi.org/10.1016/j.molonc.2013.08.010.
[22] R.M. Caprioli, T.B. Farmer, J. Gile, Molecular imaging of biological samples: localization of peptides and proteins using MALDI-TOF MS, Anal. Chem. 69 (1997) 4751–4760, https://doi.org/10.1021/ac970888i.
[23] T. Alexandrov, Spatial metabolomics and imaging mass spectrometry in the age of artificial intelligence, Annu. Rev. Biomed. Data Sci. 3 (2020) 61–87, https://doi.org/10.1146/annurev-biodatasci-011420-031537.
[24] T.J.A. Dekker, E.A. Jones, W.E. Corver, R.J.M. van Zeijl, A.M. Deelder, R.A.E. M. Tollenaar, W.E. Mesker, H. Morreau, L.A. McDonnell, Towards imaging metabolic pathways in tissues, Anal. Bioanal. Chem. 407 (2015) 2167–2176, https://doi.org/10.1007/s00216-014-8305-7.
[25] K.V. Djambazova, D.R. Klein, L.G. Migas, E.K. Neumann, E.S. Rivera, R. Van de Plas, R.M. Caprioli, J.M. Spraggins, Resolving the complexity of spatial lipidomics using MALDI TIMS imaging mass spectrometry, Anal. Chem. 92 (2020) 13290–13297, https://doi.org/10.1021/acs.analchem.0c02520.
[26] B. Martin, J.P.L. Gonçalves, C. Bollwein, F. Sommer, G. Schenkirsch, A. Jacob, A. Seibert, W. Weichert, B. Märkl, K. Schwamborn, A mass spectrometry imaging based approach for prognosis prediction in UICC stage I/II colon cancer, Cancers 13 (2021) 5371, https://doi.org/10.3390/cancers13215371.
[27] S. Shimma, Y. Sugiura, T. Hayasaka, Y. Hoshikawa, T. Noda, M. Setou, MALDI-based imaging mass spectrometry revealed abnormal distribution of phospholipids in colon cancer liver metastasis, J. Chromatogr., B: Anal. Technol. Biomed. Life Sci. 855 (2007) 98–103, https://doi.org/10.1016/j.jchromb.2007.02.037.
[28] A. Thomas, N.H. Patterson, M.M. Marcinkiewicz, A. Lazaris, P. Metrakos, P. Chaurand, Histology-driven data mining of lipid signatures from multiple imaging mass spectrometry analyses: application to human colorectal cancer liver metastasis biopsies, Anal. Chem. 85 (2013) 2860–2866, https://doi.org/10.1021/ac3034294.
[29] Z. Pang, G. Zhou, J. Ewald, L. Chang, O. Hacariz, N. Basu, J. Xia, Using MetaboAnalyst 5.0 for LC-HRMS spectra processing, multi-omics integration and covariate adjustment of global metabolomics data, Nat. Protoc. 17 (2022) 1735–1761, https://doi.org/10.1038/s41596-022-00710-w.
[30] D.S. Wishart, A. Guo, E. Oler, F. Wang, A. Anjum, H. Peters, R. Dizon, Z. Sayeeda, S. Tian, B.L. Lee, M. Berjanskii, R. Mah, M. Yamamoto, J. Jovel, C. Torres-Calzada, M. Hiebert-Giesbrecht, V.W. Lui, D. Varshavi, D. Varshavi, D. Allen, D. Arndt, N. Khetarpal, A. Sivakumaran, K. Harford, S. Sanford, K. Yee, X. Cao, Z. Budinski, J. Liigand, L. Zhang, J. Zheng, R. Mandal, N. Karu, M. Dambrova, H.B. Schiöth, R. Greiner, V. Gautam, Hmdb 5.0: the human metabolome database for 2022, Nucleic Acids Res. 50 (2022) D622–D631, https://doi.org/10.1093/nar/gkab1062.
[31] C. Ruttkies, E.L. Schymanski, S. Wolf, J. Hollender, S. Neumann, MetFrag relaunched: incorporating strategies beyond in silico fragmentation, J. Cheminf. 8 (2016) 3, https://doi.org/10.1186/s13321-016-0115-9.
[32] L.W. Sumner, A. Amberg, D. Barrett, M.H. Beale, R. Beger, C.A. Daykin, T.W.-M. Fan, O. Fiehn, R. Goodacre, J.L. Griffin, T. Hankemeier, N. Hardy, J. Harnly, R. Higashi, J. Kopka, A.N. Lane, J.C. Lindon, P. Marriott, A.W. Nicholls, M.D. Reily, J.J. Thaden, M.R. Viant, Proposed minimum reporting standards for chemical analysis chemical analysis working group (CAWG) metabolomics standards initiative (MSI), metabolomics off, J. Metabolomic Soc. 3 (2007) 211–221, https://doi.org/10.1007/s11306-007-0082-2.
[33] A. Nilsson, A. Peric, M. Strimfors, R.J.A. Goodwin, M.A. Hayes, P.E. Andrén, C. Hilgendorf, Mass Spectrometry Imaging proves differential absorption profiles of well-characterised permeability markers along the crypt-villus axis, Sci. Rep. 7 (2017) 6352, https://doi.org/10.1038/s41598-017-06583-4.
[34] I. Dabaj, J. Ferey, F. Marguet, V. Gilard, C. Basset, Y. Bahri, A.-C. Brehin, C. Vanhulle, F. Leturcq, S. Marret, A. Laquerrière, I. Schmitz-Afonso, C. Afonso, S. Bekri, A. Tebani, Muscle metabolic remodelling patterns in Duchenne muscular dystrophy revealed by ultra-high-resolution mass spectrometry imaging, Sci. Rep. 11 (2021) 1906, https://doi.org/10.1038/s41598-021-81090-1.
[35] Z. Zhou, J. Tu, X. Xiong, X. Shen, Z.-J. Zhu, LipidCCS: prediction of collision cross-section values for lipids with high precision to support ion mobility-mass spectrometry-based lipidomics, Anal. Chem. 89 (2017) 9559–9566, https://doi.org/10.1021/acs.analchem.7b02625.
[36] S. Taira, M. Hashimoto, K. Saito, O. Shido, Visualization of decreased docosahexaenoic acid in the hippocampus of rats fed an n – 3 fatty acid-deficient diet by imaging mass spectrometry, J. Biophys. Chem. 3 (2012) 221–226, https://doi.org/10.4236/jbpc.2012.33025.
[37] G. Sighinolfi, S. Clark, L. Blanc, D. Cota, B. Rhourri-Frih, Mass spectrometry imaging of mice brain lipid profile changes over time under high fat diet, Sci. Rep. 11 (2021) 19664, https://doi.org/10.1038/s41598-021-97201-x.
[38] S. Miyamoto, C.-C. Hsu, G. Hamm, M. Darshi, M. Diamond-Stanic, A.-E. Declèves, L. Slater, S. Pennathur, J. Stauber, P.C. Dorrestein, K. Sharma, Mass spectrometry imaging reveals elevated glomerular ATP/AMP in diabetes/obesity and identifies sphingomyelin as a possible mediator, EBioMedicine 7 (2016) 121–134, https://doi.org/10.1016/j.ebiom.2016.03.033.
[39] Q. Zhang, Z.-H. Wu, S.-S. Zhao, J. Yang, L. Chen, X.-Y. Wang, Z.-Y. Wang, H.-X. Liu, Identification and spatial visualization of dysregulated bile acid metabolism in high-fat diet-fed mice by mass spectral imaging, Front. Nutr. 9 (2022). https://www.frontiersin.org/articles/10.3389/fnut.2022.858603. (Accessed 5 October 2022).
[40] E.R. Guiberson, C.J. Good, A.G. Wexler, E.P. Skaar, J.M. Spraggins, R.M. Caprioli, Multimodal imaging mass spectrometry of murine gastrointestinal tract with retained luminal content, J. Am. Soc. Mass Spectrom. 33 (2022) 1073–1076, https://doi.org/10.1021/jasms.1c00360.
[41] L.R.S. Huizing, J. McDuffie, F. Cuyckens, M. Heerden, T. Koudriakova, R.M. A. Heeren, R.J. Vreeken, Quantitative mass spectrometry imaging to study drug distribution in the intestine following oral dosing, Anal. Chem. 93 (2021) 2144–2151, https://doi.org/10.1021/acs.analchem.0c03956.
[42] D. Furth-Walker, N.K. Amy, Regulation of xanthine oxidase activity and immunologically detectable protein in rats in response to dietary protein and iron, J. Nutr. 117 (1987) 1697–1703, https://doi.org/10.1093/jn/117.10.1697.
[43] P. Ji, E. B Nonnecke, N. Doan, B. Lönnerdal, B. Tan, Excess iron enhances purine catabolism through activation of xanthine oxidase and impairs myelination in the Hippocampus of nursing piglets, J. Nutr. 149 (2019) 1911–1919, https://doi.org/10.1093/jn/nxz166.
[44] A.J. Ghio, T.P. Kennedy, J. Stonehuerner, J.D. Carter, K.A. Skinner, D.A. Parks, J. R. Hoidal, Iron regulates xanthine oxidase activity in the lung, Am. J. Physiol. Lung Cell Mol. Physiol. 283 (2002) L563–L572, https://doi.org/10.1152/ajplung.00413.2000.
[45] J. Keller, S. Chevolleau, M.-H. Noguer-Meireles, E. Pujos-Guillot, M. Delosière, C. Chantelauze, C. Joly, F. Blas-Y-Estrada, I. Jouanin, D. Durand, F. Pierre, L. Debrauwer, V. Theodorou, F. Guéraud, Heme-iron-induced production of 4-hydroxynonenal in intestinal lumen may have extra-intestinal consequences through protein-adduct formation, Antioxid. Basel Switz. 9 (2020) E1293, https://doi.org/10.3390/antiox9121293.
[46] O.C.B. Martin, N. Naud, S. Taché, L. Debrauwer, S. Chevolleau, J. Dupuy, C. Chantelauze, D. Durand, E. Pujos-Guillot, F. Blas-Y-Estrada, C. Urbano, G.G. C. Kuhnle, V. Santé-Lhoutellier, T. Sayd, D. Viala, A. Blot, N. Meunier, P. Schlich, D. Attaix, F. Guéraud, V. Scislowski, D.E. Corpet, F.H.F. Pierre, Targeting colon luminal lipid peroxidation limits colon carcinogenesis associated with red meat consumption, Cancer Prev. Res. Phila. Pa 11 (2018) 569–580, https://doi.org/10.1158/1940-6207.CAPR-17-0361.
[47] P. Steinberg, Red meat-derived nitroso compounds, lipid peroxidation products and colorectal cancer, Foods Basel Switz. 8 (2019) E252, https://doi.org/10.3390/foods8070252.
[48] K. Yamamoto, S. Higashi, M. Kioi, J. Tsunezumi, K. Honke, K. Miyazaki, Binding of active matrilysin to cell surface cholesterol sulfate is essential for its membrane-associated proteolytic action and induction of homotypic cell adhesion, J. Biol. Chem. 281 (2006) 9170–9180, https://doi.org/10.1074/jbc.M510377200.
[49] S. Higashi, M. Oeda, K. Yamamoto, K. Miyazaki, Identification of amino acid residues of matrix metalloproteinase-7 essential for binding to cholesterol sulfate, J. Biol. Chem. 283 (2008) 35735–35744, https://doi.org/10.1074/jbc.M806285200.